



CHAPTER 2 Possible role of blood cells in differential wound healing of lizard appendages

INTRODUCTION

Induction of autotomy or surgical amputation of appendage exposes the inner sterile tissues to a plethora of foreign entities, making the subject vulnerable to microbial attack and infections. Thus, the preliminary job of the exposed tissue is to ensure sealing of wound (Arrington and Miller, 1995). Epidermal and mesenchymal cells participate in the repair process to heal the wound (Simkin et al., 2015). Further, COX-2 derived PGE₂ and the recruited chemical mediators of inflammation devise the route of differential wound healing in lizard appendages (Khaire et al., 2021). These chemicals are primarily secretions of local cells present at the site of injury or they arrive at the spot along with the blood flow. The blood vessels spread in the region, bring all the necessary ingredients to the wound site based on the triggers sent by the injured tissue (Gonzalez et al., 2016).

Predominantly, cells such as neutrophils and macrophages send molecular signals to recruit other important cell types at the site of healing (Rosales, 2018). The entire trail of event is a function of strictly regulated, concentration dependent action of chemokines (Nauseef and Borregard, 2014). All cells responding to these chemicals reach the wound arena and get modified to expedite the process of repair.

Inflammation and Amendments: What do blood cells do?

In the present case of lizard appendages, the wounds inflicted are different in both tail and limb. Lizard tail is ingeniously designed to allow 'easy' and relatively less invasive release of appendage. Owing to the pre-fractured architecture, there is minimal or no blood loss after inducing autotomy (Vitt, 1983; Sharma and Suresh, 2008). As observed through morphometry described in Chapter 1, expeditious wound closure occurs by the end of the first 24 hours post-autotomy. Followed by which, a visible wound epithelium is formed by 4dpa. These stages of repair are instigated by the cellular cues, especially from the vascular systems (Xu et al., 2019). Other tissues such as muscles, bones etc are more 'bundled' and arranged in a juxtaposed manner under the blanket of adipocytes and skin (Sanggaard et al., 2012).

Post-injury response is somewhat subtle in lizard tail, as a result of which the course and spread of inflammation are alleviated pretty quickly from the tissue environment. On the limb front though, a massive injury caused due to amputation leads to a scabby and unrefined scar formation, in a time frame of more than 12 days (Alibardi, 2009; Ranadive et al., 2018). Herein, substantial blood loss follows amputation and a thick blood clot is formed, which blocks any major cellular migration as otherwise seen in tail. This resulting clot is a desperate effort of the appendage to block entry of any pathogens. The tissue rupture caused due to severing of an appendage, releases a wide range of cytokines increasing inflammation at the site of injury (Cameron and Kelvin, 2000).

It is crucial to note that the response to injury is diagonally opposite in tail and limb and so is the repair outcome. There appear a lot of unanswered questions, for an instance: If blood loss is minimal, and inflammation is on the receding side in tail, which cells perform the imperative pro-repair signalling relay? How is the repair machinery induced differentially in tail and limb? Does pool of blood at the wound site play reformatory or restraining role in limb healing? All these questions prompted us to check the status of various cells of blood and their effects on repair process, which is disparately patterned in tail and limb. As highlighted in General Introduction section, inflammation is a collaborative outcome of cells and cytokines in blood circulation. With this information in hand, we explored the blood cells circulating through the vasculature of lizards. The idea was simple, as we have discovered the altering course of inflammation through the interleukin window, now was the turn to observe the temporal status of blood cells, their arrival at the locale of action and plausible function as well.

Being a vertebrate, lizards possess a closed circulatory system much similar to mammals (Shah et al., 1978; Campbell, 2015). What is exciting and equally challenging in this system are some specific cell types, which are not found in mammals. The cells present in lizards are designed to address any challenges posed by external agents but their efficiency is limited as compared to the mammalian blood cells. As we have seen earlier, reptiles rely largely on the innate immunity and the adaptive nature of this system is apparently less developed (Rios and Zimmerman, 2015). This is evident from the cell types and their titer at the healing site.

Blood cells in lizards

A survey through the literature revealed the presence of erythrocytes, heterophils, eosinophils, basophils, lymphocytes, monocytes and macrophages in various species of lizard. A brief description of their unique features is annotated below.

Erythrocytes

Unlike mammalian erythrocytes, the ones present in lizards are relatively larger, ellipsoid and nucleated in nature (Saldanha and Silva-Herdade, 2017). Various types of erythrocytes are classified based on chromatin composition, age of the organism etc (Nayak and Mohanty, 2020). They stain light pink with a dense purple coloured nucleus at the centre in mature erythrocytes, while the immature ones have relatively lighter centre (Sykes and Klaphake, 2008). Non-mammalian nucleated erythrocytes are known to carry PRRs which enable them to participate in PAMP specific response, further confirming their direct participation in immune response (Morera and MacKenzie, 2011).

Heterophils

Heterophils and eosinophils are the two discernible members of acidophilic granulocyte family. Their nuclear structure is round to oval while lizards have predominantly multilobed nucleus in heterophils (Montali, 1988). Functionally, heterophils are similar to mammalian neutrophils, but they primarily use oxygen-independent machinery to destroy pathogens in lizards (Montali, 1988).

Eosinophils

Eosinophils have an eccentric nucleus and numerous cytoplasmic granules. Their size and numbers are highly variable in all reptiles (Campbell, 2015). Specific surface markers are needed to differentiate heterophils from eosinophils as the basic staining techniques leave no such possibility. In reptiles, role of eosinophils in manifestation of inflammation is not clear yet, while in other vertebrates such as birds and mammals, these cell types are directly associated with hypersensitivity and combatting helminth infections (Chusid, 2018).

Basophils

They are smaller than both heterophils and eosinophils, with a variable number of round metachromatic cytoplasmic granules. Lizards particularly have smaller basophils which increase in size under toxic changes, generally leading to a basophilia (Campbell, 2004).

Lymphocytes

Nuclear chromatin in lymphocytes is highly condensed in reptiles similar to aves and mammals. Also, the centrally placed nucleus might possess granules observed in Wright-Giemsa staining. Lymphocytes are attributed with the similar functions as in birds, wherein they elicit the primary immune response (Claver and Quaglia, 2009).

Monocytes & Macrophages

Oval, round or bean shaped nucleus is a marker of reptilian monocyte. Similar to their mammalian counterpart, monocytes in lizards are predominantly concerned with phagocytic activity and are precursors to macrophagic population (Rooney, 2005). A special feature of reptilian monocytes is the presence of azurophilic granules, and hence they are known as azurophilic monocytes (Ghorai and Priyam, 2018).

Both tissue resident as well as circulating macrophages release a large number of cytokines which alter the levels of inflammation (Nardini et al., 2014). Identifying active monocytes and macrophages may provide maximum insight on inflammation and its effect on wound healing. Hence, all experiments were strategized with an aim to highlight roles of monocytes and macrophages in controlling inflammation and resultant wound healing in the two appendages.

Thrombocytes

Reptilian thrombocytes appear to be fusiform in shape with dense nuclear chromatin placed in the centre. They are generally found in clusters and function similar to human platelets. They too form thrombus and regulate clot formation process (Weyrich et al., 2003; Yokoyama, 2008). In times of acute inflammation, polymorphic nuclei are found in

thrombocytes. In fact, thrombocyte enriched plasma has been used to promote tissue repair in chelonian models (Weyrich et al., 2003).

Owing to the many similarities in structure and function of reptilian and mammalian blood cells, it was important to decipher plausible roles of these cells in imparting tissue specific inflammatory response, which certainly affects the wound healing events in the longer runs. In order to observe the cell types involved in inflammation and wound healing, various methods were envisaged but only few could prove handy.

Systemic blood profile

Impact of injury reflects in the leukocyte cell population and the alteration in their numbers is a real time indicator of ongoing phase of healing. Cells such as heterophils, macrophages, platelets etc., are recruited in a predetermined chronology to facilitate specific healing processes. Also, their numbers would indicate the intensity of a particular response (Kolaczowska and Kubes, 2013). Meanwhile, induced autotomy and amputation of an appendage, both lead to inflammation but at variable intensities. In order to check the status of inflammation caused by these injuries, systemic blood profile was prospected.

Challenges faced and catering approaches

Systemic blood was collected from the test animals at the defined stages of wound healing in both tail (0, 1, 2, 3 and 4dpa) and limb (0, 3, 6 and 9dpa). Blood collection was carried out under deep hypothermic condition through heart puncture method, sacrificing three animals (prepared three technical replicates from each subject) for each stage of observation.

A fixed volume of blood is not procured from these animals owing to their small body size and smaller heart chambers. Hence, instead of opting for haemocytometer-based analysis, blood smears were prepared and stained with Wright Giemsa stain (1:40). Details of slide preparation are mentioned in Materials and Methods section. Estimated total WBC count method was employed after considering all the pros and cons of this technique.

We used this overall blood counting method which establishes their “ballpark” trend through the course of wound healing. Formula for calculation of estimated WBC is mentioned in the Materials and Methods section of this chapter.

The observations are discussed at length in result section but in a gist, systemic blood count could not provide any conclusive information. Humoral profile, on the other hand showed tissue specific variation in interleukin expression in tail and limb groups (Chapter 1). Hence, we planned to check the leukocyte status at a tissue specific level.

A prerequisite for achieving this objective, was to procure blood from both, tail and limb, immediately after injury is caused. A perplexing situation arrived though, while trying to collect blood from autotomised tail as the blood loss in tail is absolutely minimal or absent (Figure 2.1).



Figure 2.1: Frontal view of lizard tail immediately post-autotomy

Knotkova et al, (2002) and other research groups have tried to investigate the reptilian hemopoiesis and blood parameters in past. For such investigations ventral puncture in the central caudal vein has been performed to retrieve blood. This method was also practically impossible with the relatively small size of the animal. Thus, the small droplets of blood were immediately used to make smears in case of tail. Nevertheless, limb tissue posed no apparent dearth of blood sample as even after deep hypothermia, some blood would ooze out from wounded region. Nonetheless, with a very low and variable amount of blood available, conducting any enzymatic analysis was not possible.

Another inevitable fact was the collaboration of tissue resident and circulating titre of immune cells, which together govern the status of inflammation and the overall immune

response. Tissue resident cells can govern all the post-amputation unfolding, and not knowing their status through the course of wound healing would keep a major loophole while evaluating the roles of leukocyte in differential wound healing. In order to avoid such complexities, one required a different approach which would eradicate the discrepancies created amongst the two tissue systems. Hence, Fluorescence Activated Cell Sorting (FACS) was attempted on the harvested tissues (both tail and limb).

FACS: A plausible saviour

Fluorescence activated cell sorting, is a sophisticated flow cytometric technique which has a wide spectrum of usage and sensitivity to scale up a single cell from large clusters (Wilkerson, 2012). The science behind this high throughput technique, relies on the optical and fluorescent characters of cells, particles, chromosomal preparation etc that are subjected to a light source (Macey, 2007). Scattering of the incident light is a function of granularity, position, density and size of the matter passing through the light beam. Hence cluster of cells can be differentiated and sorted based on the specific combination of these above-mentioned features along with the overall morphology of cells (Reggeti and Bienzle, 2011). On the other hand, fluorescence measured through this technique is attributed to specific fluorescent probes attached to the cell surface, which are excited to emit specific wavelengths (Wilkerson, 2012). The following discussion will emphasize the cell sorting procedures considering the purpose and focus of present study.

Being an advanced version of flow cytometry, FACS is comprised of two systems:

i. Fluidics (Direction, medium and path of fluids)

Cells are allowed to pass through the light beam in a specific fluid medium which is known as the sheath fluid which works as a diluent too (Adan et al., 2017). Generally, PBS suffices this purpose and is injected in the flow chamber under well-regulated pressure. Cells are also injected through pressurized air lines, constituting the sample stream. Pressure difference between the sheath fluid and sample stream ensures single cell alignment in the flow chamber. Thus, through hydrodynamic focussing, assessment of every cellular entity is made in FACS machine (Adan et al., 2017).

ii. Optics (Excitation and Emission)

Excitation and emission of high energy photons characterize and classify various cell types, differentially. Lasers and lenses constitute the core of optics, providing the light source and specific directional focus, respectively. When photon beam collides with the cells, light scatters based upon size, density, nucleus, granularity, shape and surface topology of the cell in focus. The phenomenon is known as ‘scattering’. The total light scattered can be classified in two types - forward scatter (FSC) and side scatter (SSC). Primarily, FSC is a result of diffraction along the same axis of the incident light. It strictly depends on the cell surface and size. SSC, on the other hand, represents reflected and refracted light and is collected at 90° to the incident angle (Jahan-Tigh et al., 2012; Adan et al., 2017). Proportional to the granularity and density of the cells, intensity of SSC varies from cell to cell. Every cell, based on its specific features scatters the light to give a certain range of FSC/SSC ratio (Reggeti and Bienzle, 2011).



Figure 2.2: FACS set up

Once, the cells have been subjected to FACS machine, electronic network and detectors are required to complete the circuit as they play pivotal roles in data acquisition and processing. A complete FACS setup can be seen in figure 2.2.

FACS data analysis

Gating

Cells undergo a stringent screening process as their various features like size, density, granularity, presence of surface receptors, membrane topography etc are recorded. Based on these characters, all cells are placed at a certain point on the scatter plot in form of an 'event' (Adan et al., 2017). Their location on the plot elicits all combination of features they possess. A specific region of interest was selected on this plot, a method known as 'gating' (Adan et al., 2017).

Single parameter Analysis

A histogram or single narrow peak is an illustration of single parameter-based screening or gating. All cells, positive for a particular fluorophore would be placed under a single peak, wherein the X axis stands for relative fluorescence intensity of single channel, while the Y axis denotes number of events positive for the given fluorescence (Jahan-Tigh et al., 2012). (Figure 2.3).

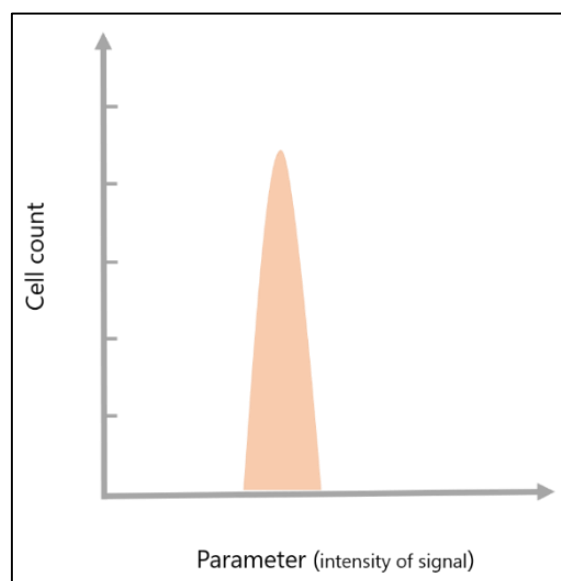


Figure 2.3: Single parameter FACS analysis plot

Two parameter Analysis

This method allows identification of cells localised on a scatter plot based on two to three parameters. The classical identification of leukocytes (granulocytes, monocytes and

lymphocytes) was performed based on the two-parameter analysis, using FSC (on X axis) and SSC intensity (on Y axis) values of the cells (Jahan-Tigh et al., 2012). These cells, further get considered for stepwise grouping and sorting.

The density plot is further divided in four quadrants (Figure 2.4). The top left quadrant (i) marks cells with highest value of SSC thus showing maximum cell granularity or complexity. Top-right quadrant (ii) indicates cell population with equally proportional FSC-SSC values, for an instance, granulocytes. Lower-right quadrant (iii) holds the cell population with larger size, though the granularity is relatively less. Monocytes make a classical illustration of such cells, with single, less granular nucleus. Both FSC and SSC values are minimal for fragmented cell debris, lying in the lower left quadrant (iv) (Adan et al., 2017).

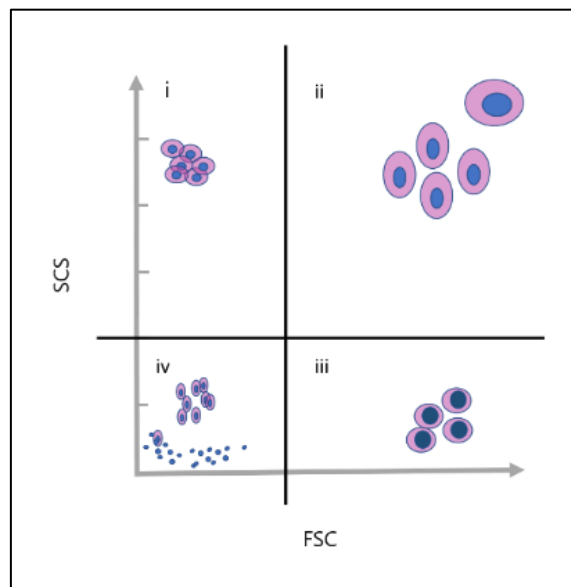


Figure 2.4: Two parameter analysis scatter plot for FACS

In case of fluorescent antibodies or dye probes used for cell identification, various combinations of parameters such as FSC-Area (FSC-A), FSC-Height (FSC-H), SSC-A, SSC-H along with the specific emission frequencies are used for cell sorting. Such combinations can be used for meticulous gating and efficient sorting of definitive cells of interest. For an instance, to obtain singlet value of cells SSC-A v/s SSC plot or FSC-A v/s FSC plot is used for both, stained or unstained cells (Herzenberg et al., 2006).

FACS: Convenient yet convoluted

Conducting FACS analysis seemed to be a promising venture as it would have provided a crisp idea of all cells present at the site of wound healing in both tail and limb. Circulating and tissue resident cells both could have been captured at differential repair sites. This would have provided vital information regarding their localisation and plausible function in the healing microenvironment.

We used FSC/SSC and fluorescent antibody probe-based cell sorting to identify all the cells belonging to myeloid lineage. Such a broad range of cells was chosen as the interconnections of all myeloid derivatives and their coherent effects on inflammation have been poorly known for *H. flaviviridis*. Cluster of differentiation (CDs) is a family of receptors present on surfaces of all leukocytes. CD-14 is specifically found on all cells of myeloid origin and hence was deployed for this study.

Working with an interesting yet a bit unusual model like *H. flaviviridis* posed few more challenges concerning the availability of specific antibodies designed for its surface markers. Hence, using antibodies designed for the closely homologous markers of other species was the only way out. Therefore, human cluster of differentiation 14 (CD-14) was used to begin this exploratory venture, owing to its presence on all myeloid cells (Zamani et al., 2013). Failure of this attempt, due to plausible species dependent variations in *H. flaviviridis* and *H. sapiens* was envisaged but a chance was taken considering a large number of conserved functions and gene sequences in lizard and human (Santonastaso, 2020). Results of this venture were interesting but not conclusive.

Tissue specific Blood Smears

As discussed earlier procuring blood was a challenging task, especially from autotomised tail regions. Herein, minimal amount of blood oozed out of the tissue. In spite of all the blood gushing out of the injured limb, equating the WBC population of tail and limb remained to be a perplexing question. Hence, we had to return to the conventional approach and estimated WBC count was performed at all healing stages of tail and limb.

MATERIALS AND METHODS

At all determined stages of wound repair, (0, 1, 2, 3 and 4dpa of tail; 0, 3, 6 and 9dpa of limb) tissue chunk of humerus region or blood was harvested. These samples were processed to either make single cell suspension (for FACS) or total WBC estimation, respectively.

FACS

Both FSC/SSC ratio and fluorescent probe-based identification of cells was carried out. Sample tissue was collected at all time points. Cells were harvested, through single cell suspension method. As a part of standardisation protocols, PBS and methanol were used for the fluidics system. The harvested tissues of 2dpa tail and 3dpa limb were used for standardisation of FACS. These time frames were specifically chosen for our pilot experiments as major inflammatory unfolding was recorded at these stages in tail and limb (Chapter 1), respectively. Details of FACS analysis are mentioned in the Materials and Methods section of thesis. The results obtained of FACS analysis prompted us to choose the latter technique of peripheral blood smears.

Total WBC estimation

Clean slides were used to make smears, which were then fixed with methanol and subjected to Wright Geimsa stain (1:40) over night. Images captured at 40x objective magnification of microscope (Leica DM2500, Germany), were used for all calculations and final estimation of total WBC from the blood smears. The formula used for calculation of estimated WBCs is as follows:

$$\text{Estimate of total WBC} = \text{Average no of WBC counted in 10 fields} \times 2000$$

All fields are captured under 40x objective lens

RESULTS

Systemic leukocyte profile: Unfazed and Unaltered

Hemidactylus flaviviridis blood smear shows numerous cell types, which have distinct phenotype but function similar to their mammalian counterparts. Morphology of these blood cells is clearly depicted in figure 2.5A-F. As mentioned in introduction of this

chapter, the cells have all the characteristic features as identified in other lizards and reptiles. Region highlighted through black square denotes the specific cell types found in various blood smears. Figure 2.5A shows a cluster of monocytes in the smear. Figure 2.5B shows a heterophil surrounded by erythrocytes, while 2.5C denotes granulated basophil. Figure 2.5D shows lymphocytes surrounded by erythrocytes while the highlighted region of figure 2.5E denotes a cluster of thrombocytes. Further, figure 2.5F shows multiple erythrocytes, with a prominent nucleus.

Systemic blood collected from the heart, showed a specific pattern of leukocyte expression across the healing frames of tail. At 0dpa tail 24293 ± 165 of total WBCs were recorded, which spiked significantly till 2dpa to reach a value of $29,247 \pm 403$ cells. Further, at 3dpa, 29800 ± 216 and at 4dpa, 28218 ± 298 cells were observed (Figure 2.6A; Table 2.1). On limb front, at 0dpa, 29249 ± 283 cells and at 3dpa stage, 33905 ± 888 of total WBCs were observed. At 6dpa, cell number rose to 49361 ± 398 , followed by a drop in cell numbers to reach a value of 31718 ± 483 cells at 9dpa (Figure 2.6B; Table 2.2). These results clarify leukocyte role in wound healing of tail. On limb front, clear hike in leukocyte number is observed at 6dpa stage, thus demarcating rise in inflammation on the systemic level, mostly due to appendage amputation. However, to pinpoint the differential cell count pertaining to specific microenvironment, tissue specific observations are crucial. The systemic WBC expression could be a representation of normalized status: an attempt to control inflammation and arrest it at the location of wound healing. Therefore, inflammatory response observed on systemic level cannot be considered conclusive for both tail and limb groups. Further, at 0dpa the total WBC count varied for tail and limb but this could be due to difference in initial volume obtained for making of smear. These not-so-convincing observations intrigued us to deploy a more sophisticated and sensitive technique FACS, results of which are discussed in the following segments.

Scattering of unstained cells of healing tail and limb

FACS analysis revealed the fundamental forward and side scattering features of both tail (2dpa) and limb (3dpa) tissue cells. Since both tissues have identical anatomical make up, the primary scatter plot based only on the FSC and SSC values of cells, looks similar for tail and limb (Figure 2.7A-F; Table 2.3 and 2.4). For this preliminary experimentation, PBS was used as fluidic system medium.

Based on the fundamental concept of FSC and SSC plot, Population 1 (P1) was defined by specific gating (Figure 2.7A; Table 2.3 and 2.4) for the unstained tail cells. Every dot seen in the graph represents an event, hereby showing cells possessing specific FSC and SSC values. Cells with least SSC and FSC values were categorically avoided in gating as fragmented bodies and debris falls in that quadrant. Same strategy was applied for observing the FSC v/s SSC scatter of unstained limb (Figure 2.7D).

FSC-A v/s FSC plot was used to observe and define the singlet population of cells for both tail (Figure 2.7B) and limb cells (Figure 2.7E). This was called Population 2 (P2). Table 2.3 and 2.4 show percentage of events classified in P1 and P2 for both tail and limb cells, based on FSC/ SSC and FSC-A/FSC plot respectively. Autofluorescence for both tail and limb cells was recorded in CD14-FITC v/s SSC (Figure 2.7C and F). 73.91 ± 2.09 % of total events fell under Population 1, while 73.14 ± 1.45 % events are grouped as Population 2 (Figure 2.7A-B; Table 2.3), highlighting the autofluorescence of these events, most plausibly cells falling under these populations. On the limb front too, 64.45 ± 2.39 % of events were grouped under Population 1 gating, while 57.68 % events were recorded under Population 2 in unstained cells experiment (Figure 2.7D-E; Table 2.4).

It is important to note that entire tissues chunks were processed and converted into single cell suspension for this analysis. In order to identify the cells participating in inflammation, more facets and criteria were applied along with FSC/SSC values. Figure 2.7 show the panel of scatter plots for the standardisation process. PBS was used in the fluidics system for this set of experiments. Table 2.3 and 2.4 specifically highlight the events recorded for all unstained cells, isolated in both tail and limb and also state the percentage of events categorised in Population 1 and 2.

CD-14 based identification of cells in healing tail and limb through FACS

The gating protocol devised during unstained cell sorting was used to further sort the populations exhibiting CD-14 surface receptor. Owing to the dearth of lizard specific antibodies, the one designed against Human CD-14 epitopes was used with FITC conjugated secondary antibody to attempt an isolation of myeloid derived cells from the lizard cell consortia. The gating setup for the unstained cells in the previous experiment was used as a pilot protocol for identifying the variable cell types. The percentage of cell

population falling under the gate was close to that observed in case of unstained cells for both tail and limb (Table 2.3 and 2.4).

Herein, for tail, 75.32 ± 1.64 % of events were gated for Population 1 when cells were subjected to only primary antibody. On limb front, for same set of experiment, 82.06 ± 1.68 % of successful events were recorded under Population 1 (Figure 2.8A and E; Table 2.3 and 2.4). Under the gate of Population 2, 69.89 ± 2.60 events were recorded for tail, while in limb group, 72.77 ± 1.06 % of events were observed (Figure 2.8B and F; Table 2.3 and 2.4). In the third gate employed on CD-14-FITC v/s SSC plot, in order to isolate any cell population positive for CD-14 expression, no events were noted for tail, while for limb, negligible 0.53 ± 0.25 % of events were noted (Figure 2.8C and G; Table 2.3 and 2.4). When the single cell suspension was subjected to both primary (CD-14 specific) and secondary (FITC conjugated) antibodies, 74.76 ± 2.24 % of events were recorded under Population 1 in tail group, while 70.68 ± 2.87 % of events fell in this gate for limb. Population 2 gate grouped around 72.16 ± 1.34 % events for tail and 63.35 ± 4.29 % events for limb. Herein, the third gate separating events under Population 3 recorded a meagre 0.15 ± 0.09 % events for tail, while 0.36 ± 0.06 % cells were entitled in this group for limb set. (Figure 2.9C; Table 2.3 and 2.4). Nevertheless, close to the y axis, a large scatter of events was observed again pointing out a high probability of dead cells or huge cell clusters and fragmented bodies being present.

This nuclear damage was further confirmed by the graph of Ho3342 v/s FSC (Figure 2.9D; 2.10D; 2.9H; 2.10H), wherein for tail, a large number of non-specific events fell very close to the axis. In limb too, a large bunch of events were placed close to origin and high on Y axis, indicating cell debris and massive clusters along with nuclear fragments present in the medium. Certainly, Ho3342 was not introduced in this limb -single cell suspension but autofluorescence generated by cell components is registered in this panel of graphs.

Cell suspensions of tail and limb were then subjected to both primary antibody (CD-14) and secondary antibody (FITC) along with Ho3342, a fluorescent dye specifically binding the nuclear entities of cell. Figure 2.10 sums up the observations made for both tail and limb cell suspensions. The scatter plot was more refined on addition of Ho3342. Under the predefined gating, for tail, 33.08 ± 3.35 % of events were recorded, while the numbers depleted for limb as compared to previous set-up, where 19.70 ± 2.37 % events were

observed under Population 1. Population 2 gate recorded 33.37 ± 1.72 % events for tail, while for limb, 20.32 ± 1.19 % events were noted. In combined presence of primary antibody, secondary antibody and Ho3342, 7.19 ± 1.06 % of events were found falling in Population 3 for tail, while limb group showed 5.16 ± 1.31 % events (Figure 2.10A-H; Table 2.3 and 2.4). This indicates improved quality of cell suspension for both tail and limb along with the distinct cell populations clustering based on their nuclear dimensions and complexity (Figure 2.10A-H).

Despite the repeated experiments and multiple trials, the results of FACS on the entire tissue chunk-based cell suspension remained inconclusive, rather elusive. Lack of lizard specific antibodies proved to bring a major lacuna in this study. Also, a greater number of standardizations and revised gating would have added to the present information on this front. This discourse and ‘not so fruitful attempts’ to isolate the myeloid cells, led us to our next venture of FACS experiments.

FACS analysis of blood cells

Blood was collected through heart puncture of a lizard after 3 days of limb amputation. Figure 2.11 illustrates the observations made using mere unstained blood cells wherein, clear clustering could be seen and three populations could be easily identified (Figure 2.11A-B and E). FSC v/s SSC plot for all unstained cells was used to locate 3 cell populations based on the size and density of nucleus. Ho3342 v/s FSC plot though elicited the events indicating autofluorescence of cells in this channel. Population 1 and Population 2 group sorted 94.65 % and 93.05 % events, respectively. In the gates defined for Granulocytes, 21.45 % of events were noted, while Lymphocyte and Monocyte gate recorded 20.59 % and 37.34 % events, respectively (Figure 2.11; Table 2.5) Majority of events were placed high on Y axis and close to origin, thus demonstrating plausible dense clusters in the medium. Similarly, single parameter plot of Ho3342 highlighted the autofluorescence exhibited by unstained cells here (Figure 2.11D).

Lack of lizard specific markers proved to be a major deficit for this set of experiments which hindered the isolation of various populations of interest. Extensive standardisation is needed for this set of experiments. In order to avoid the massive clusters observed in FACS plots, single cell suspension making should be altered as well.

Estimate of Total WBC in Tail and Limb microenvironment

Instead of calculating the exact number for each cell type, estimation of total WBCs was found suitable for comparing the blood profile of tail and limb. Since enough and constant volume of blood could not be procured from tail, total WBC count was used for this analysis as well (using blood smears for calculation). Figure 2.12 shows the panel of representative blood smears observed under 40x objective lens. These snaps were used for identifying the cell types and counting total WBCs. Blood smears made at every stage of healing i.e., 0dpa, 1dpa, 2dpa, 3dpa and 4dpa for tail and 0dpa, 3dpa, 6dpa and 9dpa of limb were used for this series of observation. Figure 2.13A-B and Table 2.6 and 2.7 comprehend the total WBC counted for both appendages. Initially, at 0dpa, $26,163 \pm 467$ leukocytes were found in tail, while limb portrayed $24,606 \pm 368$ cells at the same time point. This explains the basal level of leukocyte expression showing similar trend of expression for both tail and limb.

When the wound healing progresses in tail, increasing trend of leukocyte expression was recorded with $29,587 \pm 508$ and $31,929 \pm 544$ cells found at 1 and 2dpa stage, respectively (Figure 2.12A-E; 2.13A; Table 2.6). At 3dpa and 4dpa, in tail sequential reduction in leukocyte number is recorded with $29,495 \pm 299$ cells observed at former stage and $21,919 \pm 883$ cells counted at the latter one (Table 2.6). These cell numbers, suggest reducing trend of local inflammatory response.

In limb, a progressive 'leukocyte blast' is observed with $46,913 \pm 1634$ cells at 3dpa and $1,06,601 \pm 342$ cells at 6dpa (Figure 2.12F-I; 2.13B; Table 2.7). This is a clear indication of striking inflammatory rise in limb microenvironment. Further, at 9dpa, leukocyte number reduces to $31,104 \pm 548$ with a significant drop of more than 70,000 cells, indicating clear reduction of inflammation in the microenvironment (Figure 2.12F-I; 2.13B; Table 2.7).

Results obtained here supported our notion of leukocytes closely participating in immune response. Specifically, healing tail frames showed remarkable rise in WBCs at 2dpa wherein 31929 ± 544 cells were recorded. This trend matches with subsequent rise in cytokines as mentioned in Chapter 1. A sharp rise in number of WBCs was observed at 6dpa stage in limb (Figure 2.12; 2.13). Similar to a condition like cytokine storm, a burst

of WBCs was found in tissue microenvironment, which might drive the prolonged inflammation and lead to permanent scarring.

DISCUSSION

All chemokines and other markers of inflammation are products of cellular crosstalk between epithelial, mesenchymal and blood cells (Chazaud et al., 2014). Thus, in order to form a complete and conclusive sketch of inflammatory pattern and its impact on differential wound healing, blood cells were brought under the focal point. Reptilian blood cell types, their structure and function are largely similar to mammals, even with respect to the mechanism of action. For an instance heterophils of lizard, *Iguana iguana* have shown similar ROS activity like human neutrophils (Harr et al., 2001). Heterophil numbers are found to be closely associated with proinflammatory function in reptiles (Montali, 1988; Campbell, 2015). In non-inflammatory conditions too, the count of heterophils and other leukocytes can be high owing to the increased titre of systemic glucocorticosteroids (Zapata et al., 1992; Campbell, 2015). Meanwhile, sudden rise in numbers of leukocytes is a proven marker of inflammation and that has been observed in present case too.

Astonishingly enough, same set of cells elicit disparate attendance in the different organs studied here. Despite of them being a systemic entity, their localised expression and function are strikingly variable. Our observations pertaining to cells appearing in peripheral blood smears at healing stages of tail and limb clearly show the involvement of these cells in modulation of inflammation. Reptiles per se, have a very wavering hematologic response and thus it is equally difficult to predict (Sacchi et al., 2017).

Compared to a relatively stable cellular microenvironment as observed in mammals, reptiles get affected by small alterations in their surroundings (Zapata et al., 1992). Temperature, nutrition, age; all seem to have a cohesive impact on lizard hemogram, making it difficult to assess and analyse the same. Further species-specific effect is found amongst the reptilian clan too. Thus, asserting a reference for 'normal' values of cells and their period of expression is a critical challenge in reptiles. As inflammation and following wound healing have shown tissue specific variation in the same model, we faced many challenges in establishing the normal phenotype of these blood cells in tail and limb.

FACS is one of the most sophisticated techniques used regularly to identify and classify blood cells in a wide range of model organisms. Since the technique uses light and fluorescence to evaluate cell size and complexity, it is apt to record and sort all blood cells on the basis of distinct characters.

The classical difference in the blood cells of mammals and reptiles is the presence of nucleated RBCs in the latter. This adds on to the clustering complication as separating these cells from other nucleated leukocytes needs meticulous gating and additional sorting criteria (Chamut and Arce, 2018). Removal of non-nucleated RBCs is otherwise a primary step performed on blood cell suspensions before FACS based isolation of leukocytes.

Our goal for this study was to isolate immune cells localised in the tissue and check their temporal status across the differentially healing appendages. This added to the challenge as numerous cell populations constitute all tissues of an appendage. Thus, it was difficult to isolate immune cells based on the basic scattering technique involving FSC and SSC plot. Innumerable cells would fall in the same channels as that of leukocytes and thrombocytes on FSC v/s SSC plot; and we received similar results when unstained single cell suspension of tail and limb tissues were allowed to pass through the laser of FACS (Figure 2.7). Previously Chamut and group (2018) have reported similar issues when they attempted FACS on Taegu lizards' blood samples. Similar to our observations, populations of blood cells were observed on plot, but their sorting was not too successful.

In order to avoid the large population interference, CD-14, a specific cell surface receptor found only on myeloid progeny of cells was deployed. Being meagerly studied for its genomic nuances, lizard genome is not sequenced completely and information on its protein profile is also scanty (Zimmerman, 2020). Thus, lizard specific markers are predominantly unavailable, which left us with no option but to use homology between these reptiles and other model organisms for the present venture. We used human CD-14 antibodies for homology-based identification of myeloid derivatives in lizards. The results showed a lot of non-specific binding and large clusters, improper scatter was recorded on FSC v/s SSC and CD-14-FITC v/s SSC plot. A wider range of standardisation might help on this accord but larger volumes of resources would be needed.

Since FACS analysis gave scattered and inconclusive results, we had to turn back to conventional approaches of cell staining and counting. Since many years now, a large variety of cell stains have been developed and discussed at great lengths. We deployed the classically used Wright-Giemsa stains to observe various blood cells. Procuring blood though was again a task as tail tissue did not release any blood on autotomy. If it appeared, it was in a minimal and variable quantity. Hence, instead of exact blood counting formulas, total WBCs were estimated at every stage of healing.

As seen in figure 2.12, the images taken under 40x magnification clearly show rise in number of darkly stained leukocytes. The estimated numbers of total WBCs calculated at 2dpa tail also coincide with this observation. Humoral mediators have been recorded at the same time frames in healing tail of lizards and at 2dpa, the levels of proinflammatory mediators were found to be highest (Chapter1). The simultaneous hike in total WBC count further reinforces and strongly backs the previously made observations, where cells such as macrophages and neutrophils are directed by PGE₂ in a receptor specific action (Brecht et al., 2011). This was true for limb tissue as well. At 6dpa of healing limb, excessive cells were found in the blood smears. An alarming rise of five-fold was seen in estimated number of WBCs with the simultaneous rise in cytokines as discussed in previous chapter (Chapter 1). Also, the trend of expression hiked at 3dpa as well, a clear sign of escalating inflammation. Higher grade of experiments with detailed and meticulous standardisation regime is needed to isolate immune cells from whole tissue-single cell suspension. Meanwhile, estimated WBC calculation clarifies the sketch of microenvironment, which is hijacked by immune cells for a prolonged time in limbs, while in tail, these cells arrive for a short span. They either leave the healing location or get modified to allow reduction in inflammation.

COX-2 derived PGE₂ modulates the cellular recruitment at wound healing site, in a need-based manner (Yu and Chadee, 1998) and our observations support this idea in the present model organism. Especially, leukocytes such as macrophages, neutrophils, basophils etc are brought to the microenvironment depending on the cues provided by the healing activity (Ferrante and Leibovich, 2012). These cues are predominantly regulated by pilot modulators such as COX-2 derived PGE₂ which governs both pro and antiinflammatory response (Kalinski et al., 2012; Khaire et al., 2021), further directing either regenerative or scarred wound healing as observed in tail and limb of the lizard, respectively.

PGE₂ particularly promotes influx of neutrophils (Yu and Chadee, 1998), macrophages (Xu et al., 2019) while it alters the functions of various effector cells of immunity. The host immune system can be negatively affected by PGE₂ as it reportedly ameliorates granulocyte function too (Smith, 1992). Contrasting to its established role in promoting macrophages, PGE₂ was also found to hinder the phagocytic activity of these cells, all due to specific EP receptor functioning downstream (Ballinger et al., 2006). Based on EP1-EP3 receptor action, PGE₂ is known to induce mast cells in healing microenvironment (Nakayama et al., 2006). It also promotes production of immunosuppressive vascular endothelial growth factor and MCP-1 by mast cells, thus leading to cancer metastasis (Nakayama et al., 2006).

All the cell functions enlisted here, in coherence with the differential levels of PGE₂-EP receptor activity plausibly causes differential wound healing mechanisms as observed in lizard appendages. We have observed all different cell types found in lizards, which perform all the attributed functions similar to immune cells found in mammals. The PGE₂-EP receptor action though, is less understood for the reptilian cell types and hence offers diverse opportunities for researchers to explore.

CONCLUSION

Leukocytes plausibly mediate the differential wound healing mechanisms in the two appendages viz., the tail and limb based on COX-2 derived PGE₂ function. The varying leukocyte population recruited at the site of wound healing, in coherence with the altering interleukins might lead to either pro-regenerative environment as observed in tail or scar formation as seen in limb. However, this is a preliminary investigation which requires further experimental validations. A series of meticulous studies are still required to decode the mechanisms through which these leukocytes may steer the disparate results of wound healing in the two appendages. The experiments and results of this chapter are summarised in figure 2.14.

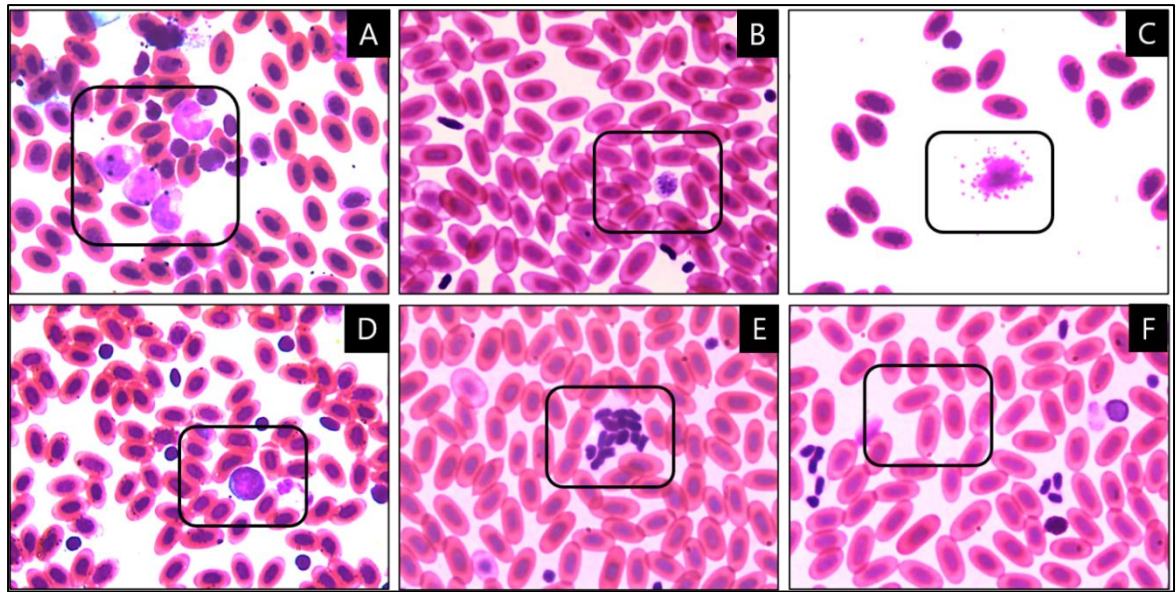


Figure 2.5: Various cell types observed in blood smear of *Hemidactylus flaviviridis*

A: Monocytes; B: Heterophil; C: Basophil with granules; D: Lymphocytes; E: Cluster of thrombocytes; F: Erythrocytes (100X objective)

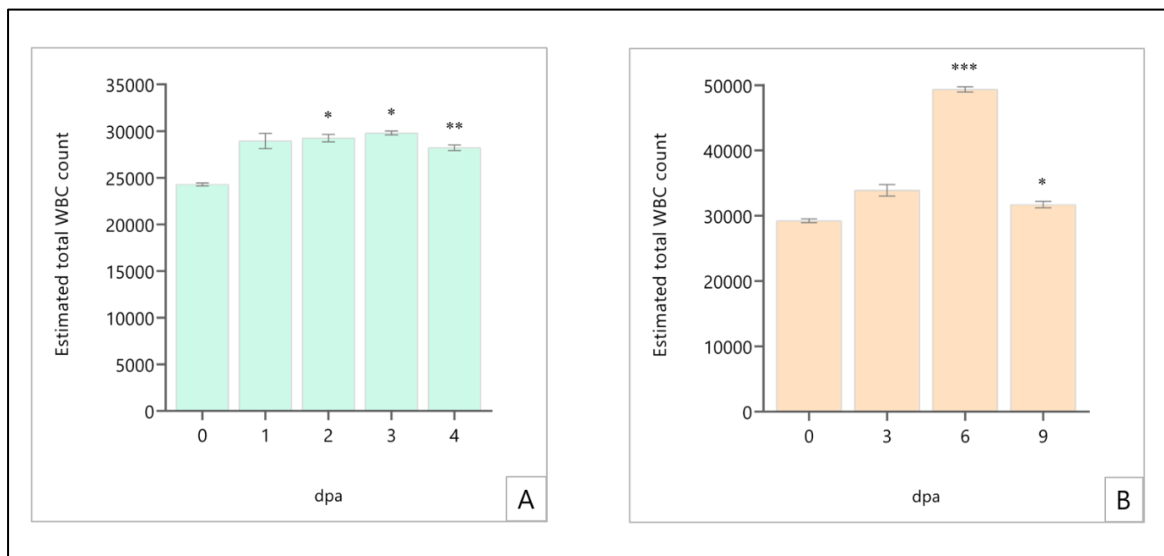


Figure 2.6: Estimated total Systemic WBCs count

A: Estimated total WBC count under autotomised tail condition; B: Estimated total WBC count under amputated limb condition. Scale bar represents SEM values. n = 6; *p<0.05, **p<0.01, ***p<0.001 as compared to 0dpa of the respective tissues.

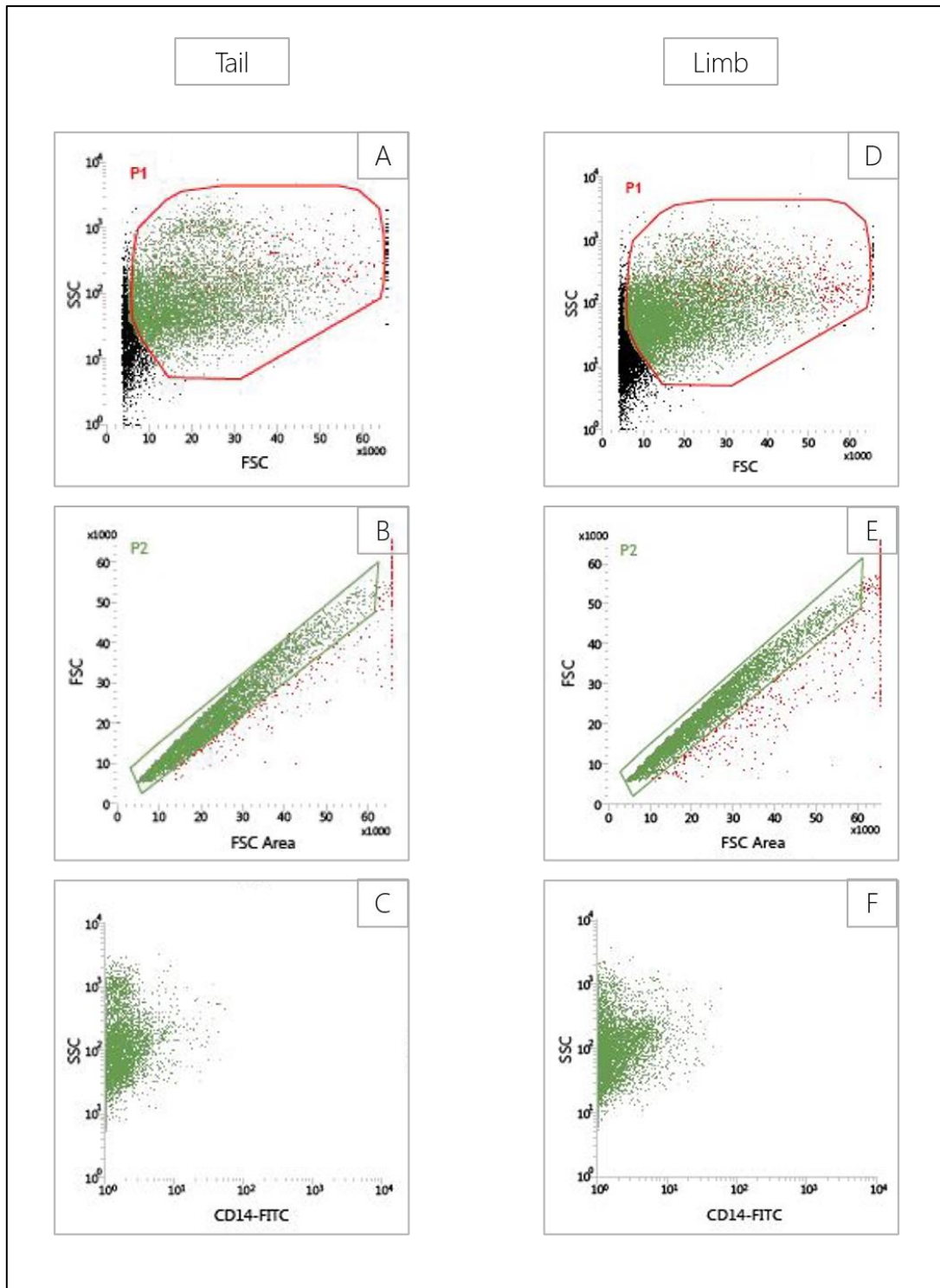


Figure 2.7: FACS analysis of cells isolated from healing tail and limb cells

A: Population 1 gating based on FSC v/s SSC scatter plot for tail cells; B: Population 2 gating based on FSC-Area v/s FSC scatter plot for tail cells; C: CD-14-FITC v/s SSC based scatter plot with majority events with high SSC values for tail cells; D: Population 1 gating based on FSC v/s SSC scatter plot for limb cells; E: Population 2 gating based on FSC-Area v/s FSC scatter plot for limb cells; F: CD-14-FITC v/s SSC based scatter plot with majority events with high SSC values for limb cells.

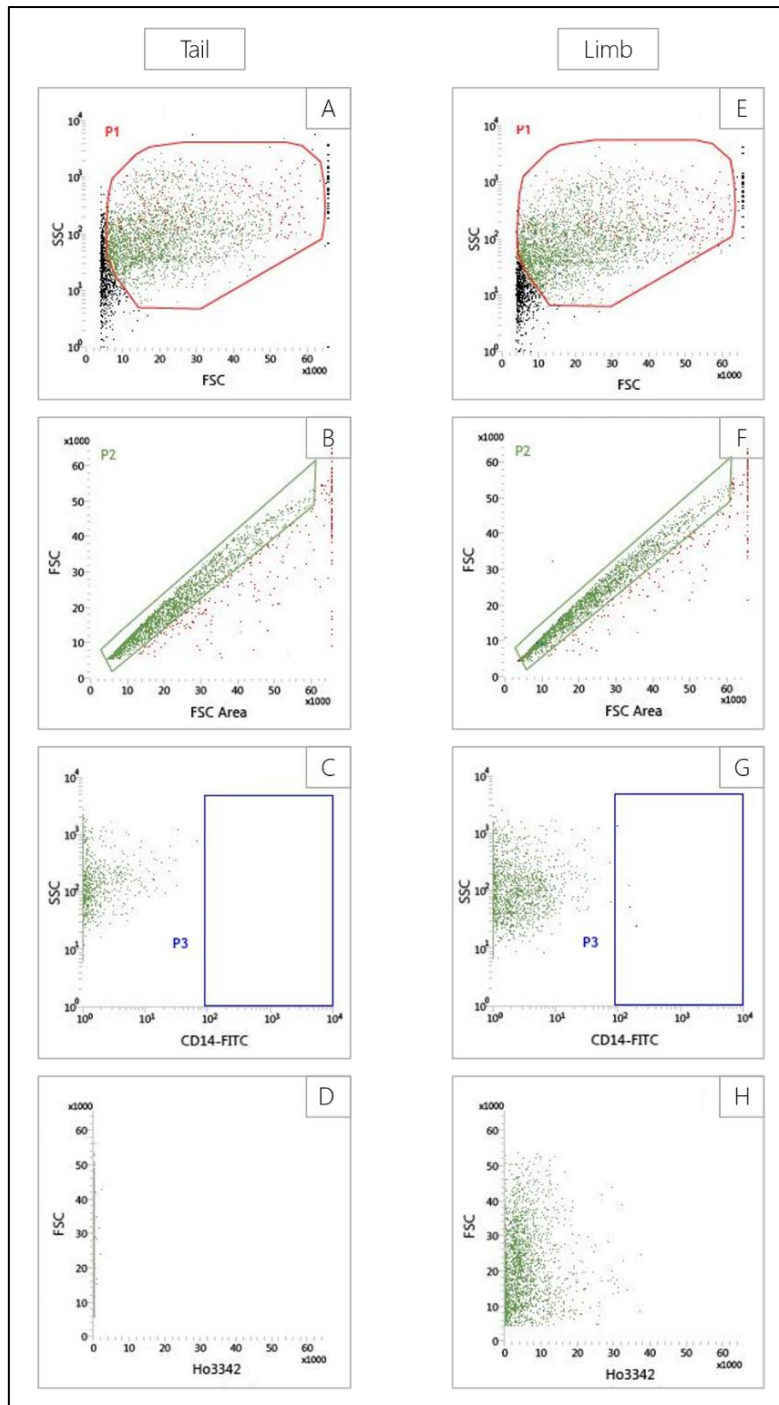


Figure 2.8: FACS analysis of tail and limb cells with primary antibody (CD-14)

A: Population 1 gating based on FSC v/s SSC scatter plot for tail cells; B: Population 2 gating based on FSC-Area v/s FSC scatter plot for tail cells; C: Population 3 gating based on CD-14-FITC v/s SSC scatter plot with majority events with high SSC values for tail cells; D: Ho3342 v/s FSC scatter plot showing autofluorescence events of tail cells; E: Population 1 gating based on FSC v/s SSC scatter plot for limb cells; F: Population 2 gating based on FSC-Area v/s FSC scatter plot for limb cells; G: CD-14-FITC v/s SSC based gating on scatter plot with majority events with high SSC values for limb cells; H: Ho3342 v/s FSC scatter plot showing autofluorescence events in limb

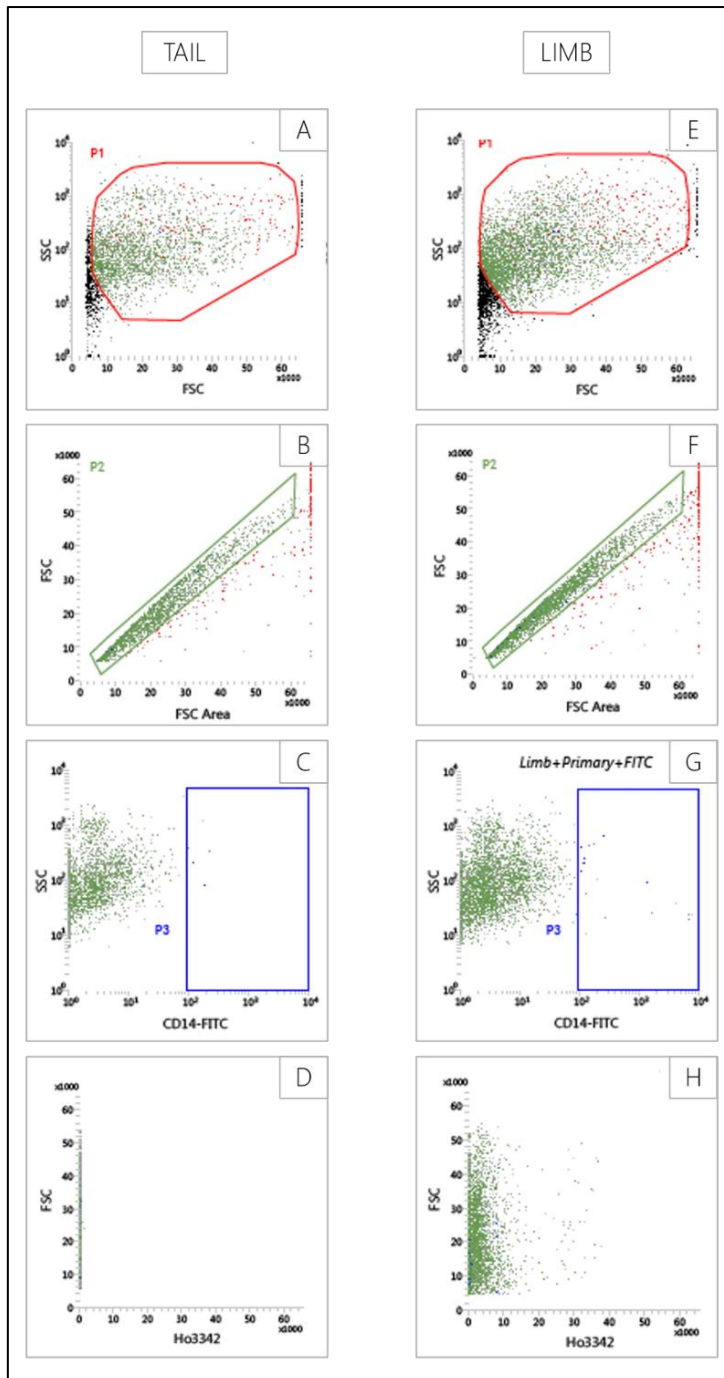


Figure 2.9: FACS analysis of tail and limb cells under CD-14-FITC probe

A: Population 1 gating based on FSC v/s SSC scatter plot for tail cells; B: Population 2 gating based on FSC-Area v/s FSC scatter plot for tail cells; C: Population 3 gating based on CD-14-FITC v/s SSC scatter plot with majority events with high SSC values for tail cells; D: Ho3342 v/s FSC scatter plot showing autofluorescence events of tail cells; E: Population 1 gating based on FSC v/s SSC scatter plot for limb cells; F: Population 2 gating based on FSC-Area v/s FSC scatter plot for limb cells; G: CD-14-FITC v/s SSC based gating on scatter plot with majority events with high SSC values for limb cells; H: Ho3342 v/s FSC scatter plot showing autofluorescence events in limb

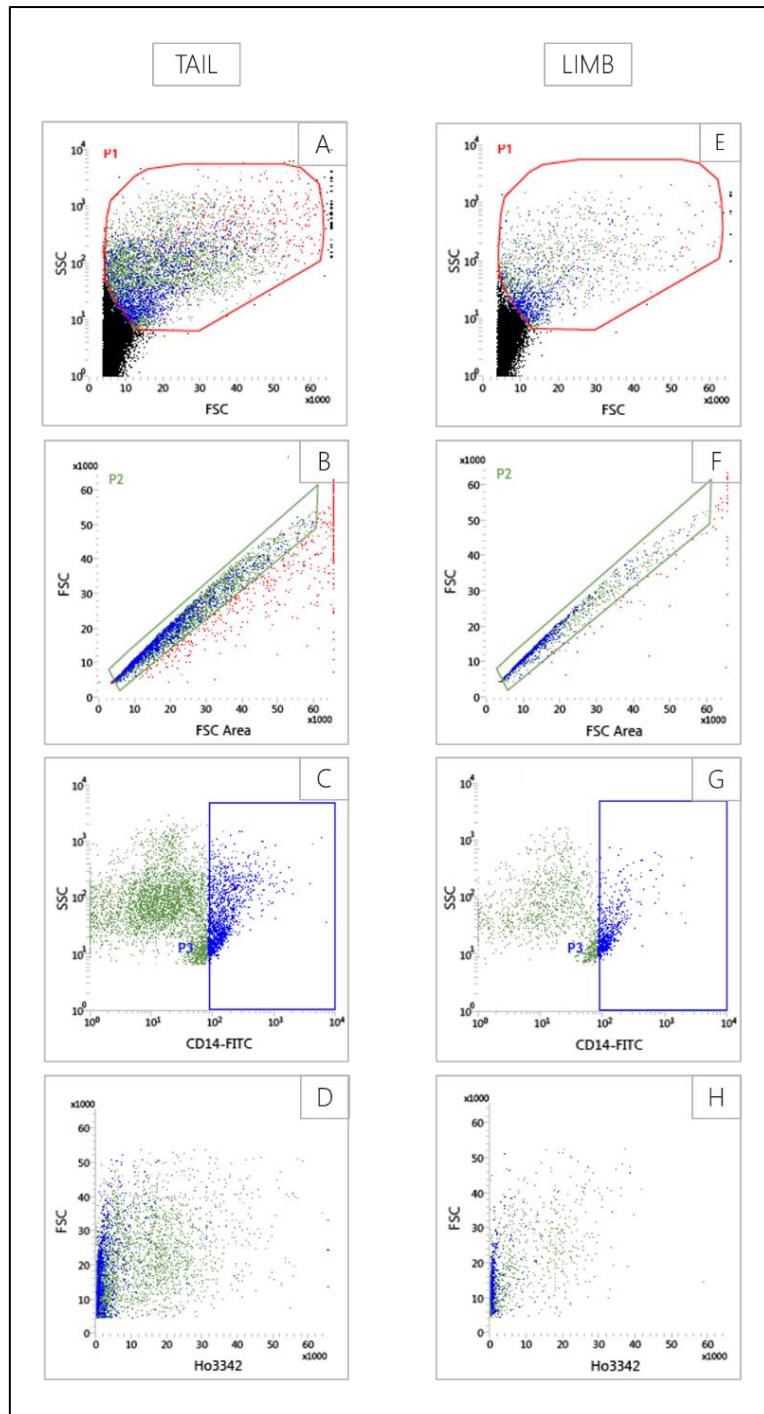


Figure 2.10: FACS analysis of tail and limb cells with CD-14-FITC and Ho3342

A: Population 1 gating based on FSC v/s SSC scatter plot for tail cells; B: Population 2 gating based on FSC-Area v/s FSC scatter plot for tail cells; C: Population 3 gating based on CD-14-FITC v/s SSC scatter plot showing positive events for tail cells; D: Ho3342 v/s FSC scatter plot showing positive events of tail cells; E: Population 1 gating based on FSC v/s SSC scatter plot for limb cells; F: Population 2 gating based on FSC-Area v/s FSC scatter plot for limb cells; G: CD-14-FITC v/s SSC based gating on scatter plot with majority events with high SSC values along with few positive events falling in the gate for limb cells; H: Ho3342 v/s FSC scatter plot showing positive events in limb cells

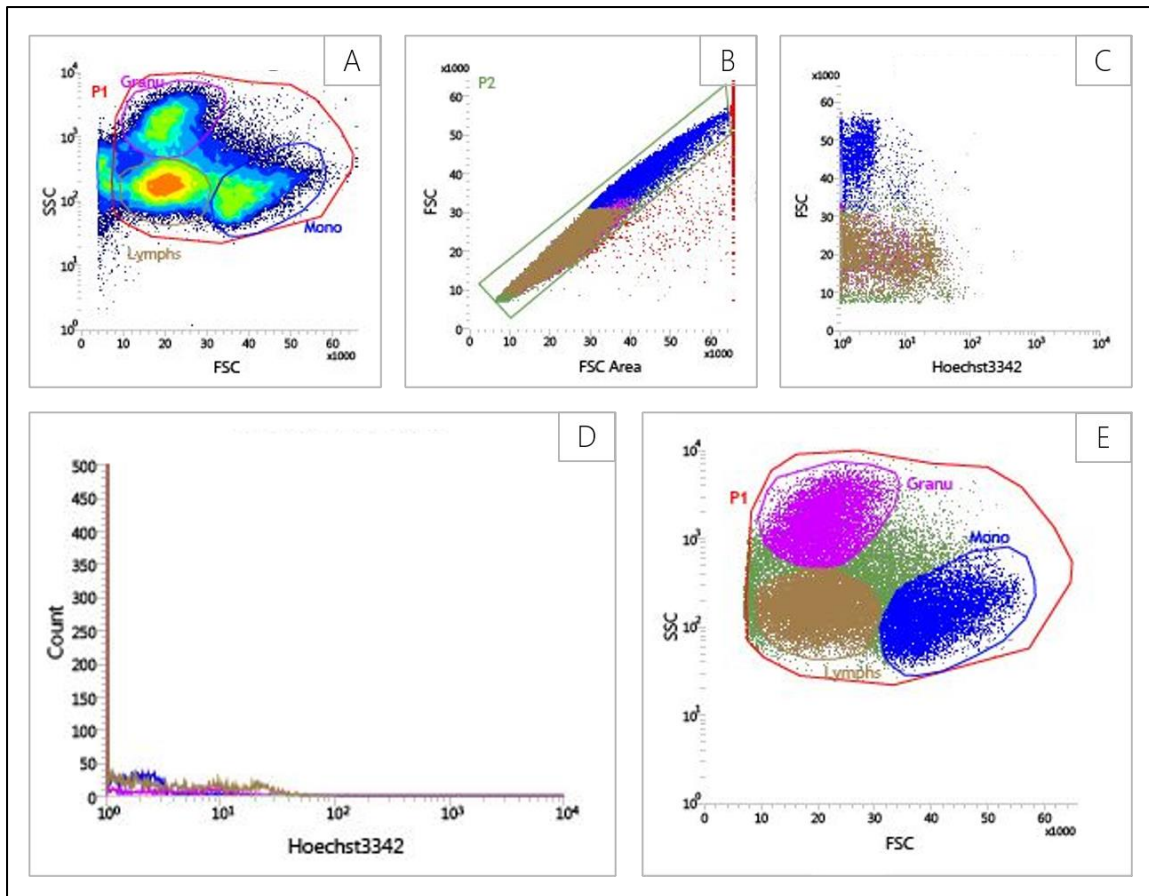


Figure 2.11: Unstained blood cells clustering in the predetermined gated channels

A: Population 1 gating based on FSC v/s SSC scatter plot for unstained blood cells; B: Population 2 gating based on FSC-Area v/s FSC scatter plot for unstained blood cells; C: Ho3342 v/s FSC scatter plot showing discrete clusters of events depicting autofluorescence of all unstained cells; D: Single parameter plot of Ho3342 showing positive events for the stain; E: Granulocyte, Monocyte and Lymphocyte gates applied to Population 1 on FSC v/s SSC scatter plot.

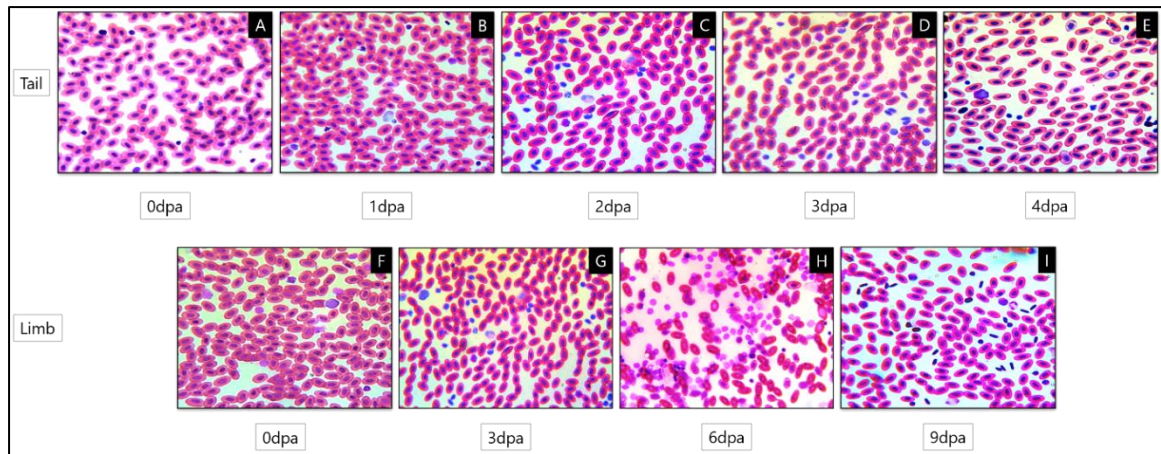


Figure 2.12: Blood cells across the healing frame of tail and limb

A-E: Tail specific blood cells stained with Wright-Giemsa stain (1:40) depicting varying leukocyte numbers at the healing stages (0, 1, 2, 3 and 4 dpa); F-I: Limb specific blood cells stained with Wright-Giemsa stain (1:40) depicting varying leukocyte numbers at the healing stages of limb (0, 3, 6 and 9 dpa) (40X Objective)

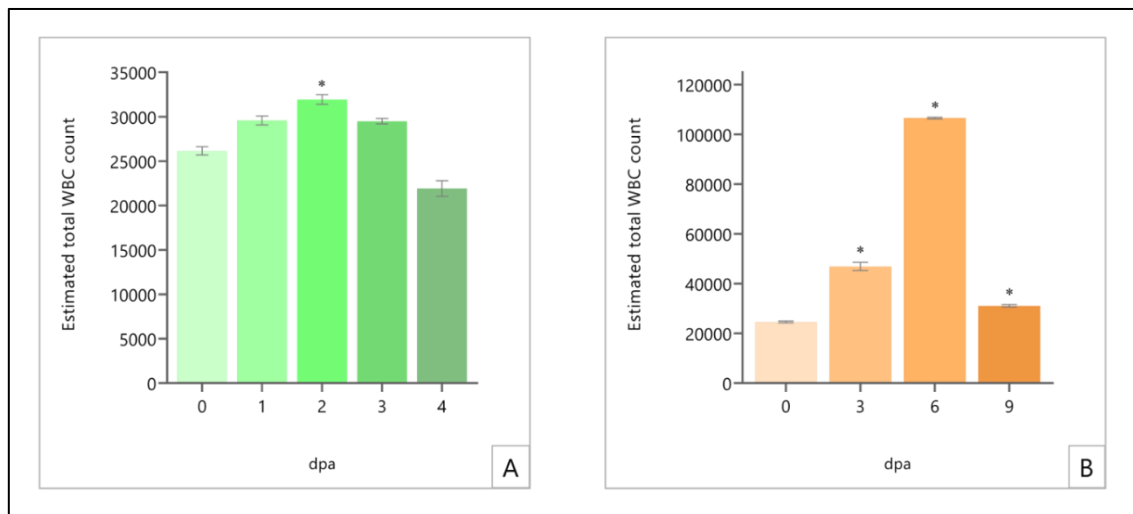


Figure 2.13: Estimated Total WBC count for A: Tail and B: Limb

Scale bar represents SEM values. n = 6; *p<0.05, as compared to 0 dpa of the respective tissues.

Systemic Estimated Total WBC (Autotomised Tail)

0dpa	1dpa	2dpa	3dpa	4dpa
24293 ± 165	28941 ± 818	29247 ± 403*	29800 ± 216*	28218 ± 298**

Table 2.1: Systemic WBC count in Autotomised Tail group

Values are expressed as Mean ± SEM; n = 6; *p<0.05, **p<0.01, as compared to 0dpa

Systemic Estimated Total WBC (Amputated Limb)

0dpa	3dpa	6dpa	9dpa
29249 ± 283	33905 ± 888	49361 ± 398***	31718 ± 483*

Table 2.2: Systemic WBC count in Amputated Limb group

Values are expressed as Mean ± SEM; n = 6; *p<0.05, ***p<0.001 as compared to 0dpa

Tail (2dpa)

P	Unstained Cells (%)	Cells+1°Ab (%)	Cells+1°Ab+2°Ab (%)	Cells+1°Ab+2°Ab+Ho33342 (%)
1	73.91 ± 2.09	75.32 ± 1.64	74.76 ± 2.24	33.08 ± 3.35
2	73.14 ± 1.45	69.89 ± 2.60	72.16 ± 1.34	33.57 ± 1.72
3	-	-	0.15 ± 0.09	7.19 ± 1.06

Table 2.3: FACS analysis of Tail (2dpa)

Values are expressed as Mean ± SEM; n = 6.

Limb (3dpa)				
P	Unstained Cells (%)	Cells+1°Ab (%)	Cells+1°Ab+2°Ab (%)	Cells+1°Ab+2°Ab+Ho33342 (%)
1	64.45 ± 2.39	82.06 ± 1.68	70.68 ± 2.87	19.70 ± 2.37
2	57.68 ± 2.46	72.77 ± 1.06	63.35 ± 4.29	20.32 ± 1.19
3	-	0.53 ± 0.25	0.36 ± 0.06	5.16 ± 1.31

Table 2.4: FACS analysis of Limb (3dpa)

Values are expressed as Mean ± SEM; n = 6.

Blood cells sorting				
Population 1 (%)	Population 2 (%)	Granulocytes (%)	Lymphocytes (%)	Monocytes (%)
94.65	93.05	21.45	20.59	37.34

Table 2.5: FACS analysis of blood

Values are expressed as Mean ± SEM; n = 6.

Tail (Estimated Total WBC)				
0dpa	1dpa	2dpa	3dpa	4dpa
26163 ± 467	29587 ± 508	31929 ± 544*	29495 ± 299	21919 ± 883

Table 2.6: Tissue specific WBC count in Tail

Values are expressed as Mean ± SEM; n = 6; *p<0.05, as compared to 0dpa

Limb (Estimated Total WBC)			
0dpa	3dpa	6dpa	9dpa
24606 ± 368	46913 ± 1634*	106601 ± 342*	31104 ± 548*

Table 2.7: Tissue specific WBC count in Limb

Values are expressed as Mean ± SEM; n = 6; *p<0.05, as compared to 0dpa

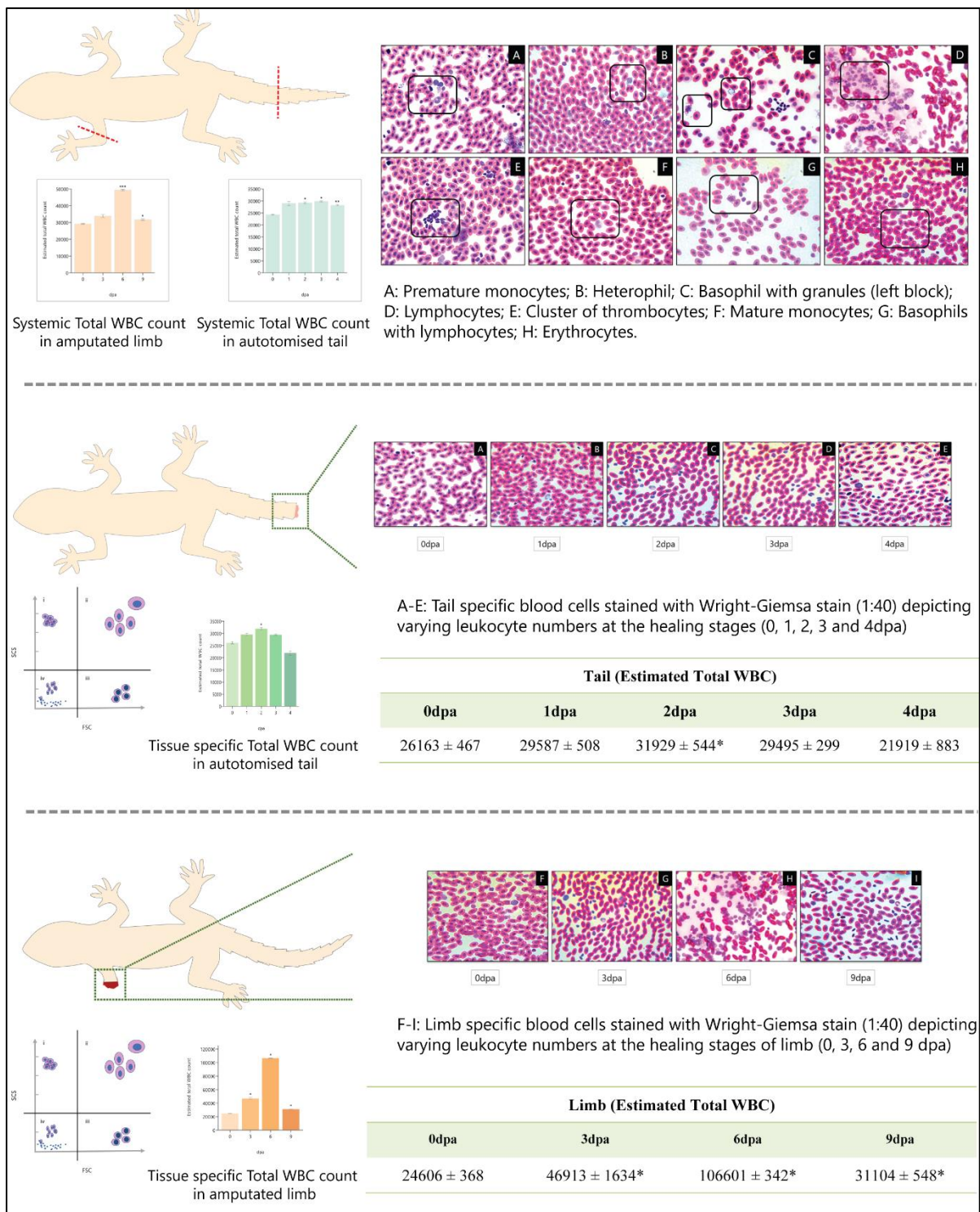


Figure 2.14: Chapter Summary